IEEE Access
Multidisciplinary ⋮ Rapid Review ⋮ Open Access Journal

Received October 30, 2020, accepted November 7, 2020, date of publication November 11, 2020,
date of current version November 20, 2020.

Digital Object Identifier 10.1109/ACCESS.2020.3037312

Adaptive EKF Based Estimation Method for Phase Noise in CO-OFDM/OQAM System

XIAOBO WANG, LIU YANG, FENGGUANG LUO, SHUAILONG YANG, AND YUTING DU
School of Optics and Electronics Information, Huazhong University of Science and Technology, Wuhan 430074, China

Corresponding authors: Liu Yang (liuyang89@hust.edu.cn) and Fengguang Luo (fgluo@hust.edu.cn)

This work was supported in part by the National Natural Science Foundation of China under Grant 62001181 and Grant 61471179, and in part by the China Postdoctoral Science Foundation funded project under Grant 2018M642843.

ABSTRACT Recently, dynamic optical network has attracted wide concern for its high efficiency and flexible configurations. Known for high spectral efficiency and flexible allocations of frequency resources orthogonal frequency-division multiplexing offset-quadrature amplitude modulation (OFDM/OQAM) is a promising scheme for future dynamic networks. Phase noise estimation (PNE) and compensation are key technologies for maintaining the performance of coherent optical OFDM/OQAM system. In this paper, a simplified phase noise (PN) model for OFDM/OQAM under channel effect is deduced according to distribution feature of intrinsic interference. Some blind PNE methods are studied and their specific implementation process for OFDM/OQAM are presented. Based on PN model and Kalman filter theory, we propose a new adaptive extended Kalman filter (AEKF) blind scheme to meet the demand of flexibility in dynamic networks. Numerical results show that AEKF can adjust the implementation complexity of PNE according to the varying laser linewidth. When the commercial laser linewidth is 200 kHz, its time complexity is only 1/3 of that of modified blind phase search with feedback loop. Besides, AEKF can achieve a stable and reliable PNE performance under varying subcarrier allocation. AEKF can achieve a stable normalized linewidth tolerance over 1.5×10^{-3} under different subcarrier allocations.

INDEX TERMS Phase noise estimation, coherent communication, orthogonal frequency division multiplexing offset quadrature amplitude modulation (OFDM/OQAM), extended Kalman Filter (EKF), flexibility.

I. INTRODUCTION

Optical network traffic has seen explosive growth over the last few decades. Fueled by a series of new technology, including internet of things and virtual reality, the communication services are gradually evolving to high capacity, high efficiency and flexible configurations. Orthogonal frequency-division multiplexing offset-quadrature amplitude modulation (OFDM/OQAM) is a promising candidate for future optical communications and has received wide concern [1]–[8]. As a multi-carrier system, OFDM/OQAM permits flexible allocations of frequency resources [1]. By using advanced filter banks, OFDM/OQAM can realize near Nyquist transmission rate and achieve higher spectral efficiency (SE) compared to orthogonal frequency-division multiplexing (OFDM) [2]. Based on the excellent time-frequency (TF) localization property of prototype filter, OFDM/OQAM can control a lower out-of-band leakage than OFDM [3]. Besides, the SE is further improved in OFDM/OQAM by canceling the necessary CP in OFDM because of the suppression of inter symbol interference and inter carrier interference (ICI) by filter bank in OFDM/OQAM [4]. However, the orthogonal conditions of OQAM only hold in real field because of the intrinsic interference (IMI) that inducing by filter banks [5]. Compared to OFDM system, OFDM/OQAM system has longer symbol duration and IMI due to filter banks. And the system performance is susceptible to laser-induced phase noise [6]–[8]. Therefore, Phase noise estimation (PNE) is indispensable and very important for application of coherent optical OFDM/OQAM (CO-OFDM/OQAM).

The objective of PNE is suppressing the effect of symbol interference induced by phase noise (PN). And it is important to analyze the characteristic and effect of PN, which has been extensively studied. In [9], [10], laser PN is modeled as a time-domain continuous Weiner process. In [11], PN effect

The associate editor coordinating the review of this manuscript and approving it for publication was Prakasam Periasamy.

in OFDM system is divided into two parts: common phase error (CPE) and ICI where CPE's effect is symbol rotation in complex domain and ICI is a Gaussian term. In [12], PN is approximated power series expansion. In [13], PN is assumed to vary linearly in the symbol duration and thus can be interpolated. In [14]–[16], PN is approximated by a set of discrete Fourier transform basis according to its low-pass nature. In [17], symbol duration is partitioned into several sub-blocks in time domain and PN in each sub-block is assumed to be constant. In [18], the Weiner model and CPE are adopted in filter bank multi-carrier (FBMC) system and CPE's effect is considered to cause a leakage of IMI on the symbol. In [19], PN's impact on bit error ratio (BER) performance is mathematically analyzed in OFDM/OQAM system. However, in practical digital signal processing (DSP), channel estimation (CE) is implemented before PNE and residual channel effect may interfere PNE performance. So far, studies have been down to analyze the PN model of OFDM/OQAM under imperfect CE.

Normally, PNE schemes can be classified into two categories according to the usage of pilot or not: pilot-aided methods and blind estimation methods. Pilot-aided methods often insert known pilot symbols into transmitted symbols to record PN [20]–[23]. For example, a PN suppression method based on orthogonal basis expansion was proposed for wireless system in [20] which supported reliable PNE at the cost of 7.3% Spectral efficiency (SE) loss. In [21], a pseudo-pilot coding based phase estimation method was proposed for coherent optical FBMC system, achieving a reliable performance at the cost of 3.1% SE loss. In [22], a pilot-based extended Kalman filter (PEKF) was proposed for coherent optical FBMC system and achieved 1.2×10^{-2} normalized linewidth (NLW) tolerance with 2.34% SE loss. In [23], a special pseudo pilot structure was proposed for FBMC system with lower SE loss of 1.2%. The pilot aided methods in [20]–[23] all cause SE loss because of pilot symbol insertion. In addition, the performance of pilot aided methods relies on high power allocation of pilot symbol which may cause power degradation of effective signal. By contrast, blind methods are popularly used for PNE without additional SE loss [19], [24]–[30]. In [24], a blind phase search (BPS) with feedback loop (BPS-FL) was proposed for OFDM system. Author in [25] proposed a modified blind phase search (MBPS) and in [26] further proposed a low complexity MBPS (LC-MBPS) in FBMC system. In [27], a BPS scheme based on dichotomy was proposed which uses a multi-stage search to reduce complexity. BPS based methods [24]–[27] all have relatively high implementation complexities due to 2-dimensional search in both symbol domain and phase domain. With proper searching set, the BPS based methods can work well under a wide NLW range at the cost of computation effort. In [28], a modified extended Kalman filter (MEKF) was proposed for offset quadrature amplitude modulation (OQAM) Nyquist wavelength division multiplexing system. Compared with BPS based methods, MEKF can only work under a low NLW with lower complexity. In [29], principal component analysis (PCA) method and PCA-BPS hybrid method were proposed to balance performance and complexity. Besides, Maximum likelihood (ML) based estimator and maximum a posteriori (MAP) based estimator were proposed in [19]. Similar to MEKF, ML and MAP estimators cannot work with large NLW. In [30], a Kullback-Leibler (KL) divergence based recursive algorithm was proposed. Complexity of KL based method is reduced by employing look up table. So far, studies have been down to explore the blind PNE methods with low complexity and high performance in OFDM/OQAM system.

In this paper, we analytically study the PN model of CO-OFDM/OQAM under fiber channel effect. According to the simplified model, we further focus on blind PNE methods and compare their performance on the basis of flexibility and complexity. Flexibility of transceiver and DSP is an important evaluation factor for dynamic networks which measures the ability to cope with varying noise, reach, spectral occupancy or other configurations [31], [32]. To my best knowledge, few studies have focused on the flexibility of PNE in OFDM/OQAM. By numerical comparison, MEKF possesses low complexity but weak flexibility while MBPS with feedback loop (MBPS-FL) has high complexity. We propose a new adaptive extended Kalman filter (AEKF) blind PNE method. AEKF scheme can adapt itself to process uncertainty to enhance stability [33], [34]. The proposed AEKF method has strong stability against varying subcarrier-allocation, channel effect and laser linewidth, thus meeting the flexibility demand in dynamic networks. Besides, AEKF has moderate lower complexity than other blind schemes mentioned.

The rest of the paper is organized as follows. In section II, the PN model of OFDM/OQAM under fiber channel effect is studied. In section III, the principles of extended Kalman filter (EKF) based blind methods are introduced and their implementation processes in OFDM/OQAM are presented. Besides, a new AEKF scheme is proposed for PNE. In section IV, the performance and complexity of different schemes are analyzed. In section V, this paper is summarized.

II. PHASE NOISE ANALYSIS IN OFDM/OQAM

The OFDM/OQAM system model is shown in Fig. 1. At the transmitter side, the transmitted bit sequence is first divided into M parallel sequences, corresponding to M subcarriers. After quadrature amplitude modulation (QAM) mapping, one complex symbol on each subcarrier is divided to two OQAM symbols which are respectively real part and imaginary part of complex symbol. Let T be the QAM symbol duration, and the OQAM symbol duration is T/2. Then by offset module, real part OQAM symbol delays for T/2 compared to imaginary part. In order to keep signal orthogonality, the OQAM symbols are multiplied with pre-built phase codes. After that, inverse fast Fourier transform and filter banks constitute the so called poly-phase network, and transform the symbols into time domain signals. The discrete time-domain modulated

TABLE 1. IMI coefficients with negative sign ignored.

	k-4	k-3	k-2	k-1	k	k+1	k+2	k+3	k+4
m-2	0	0.0006	0.0001	0	0	0	0.0001	0.0006	0
m-1	0.0054	0.0429	0.1250	0.2058	0.2393	0.2058	0.1250	0.0429	0.0054
m	0	0.0668	0.0002	0.5644	1	0.5644	0.0002	0.0668	0
m+1	0.0054	0.0429	0.1250	0.2058	0.2393	0.2058	0.1250	0.0429	0.0054
m+2	0	0.0006	0.0001	0	0	0	0.0001	0.0006	0

Neighbor number	NOIR (dB)
8	7.3
14	19.1
20	32.4

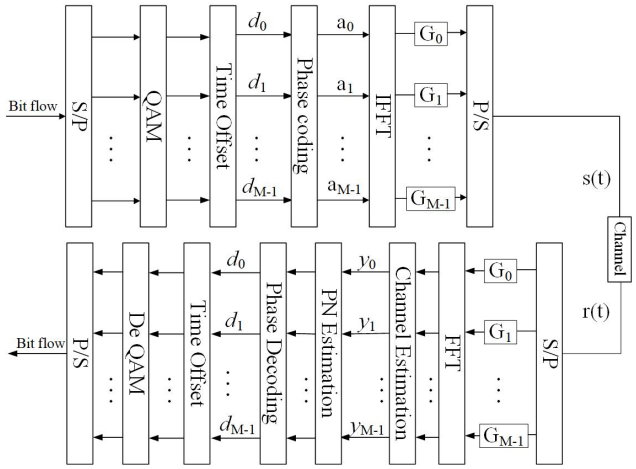

FIGURE 1. OFDM/OQAM system diagram. S/P: serial to parallel conversion. P/S: parallel to serial conversion. G_m: the m-th filter in filter bank.

signals can be expressed as:

$$s(l) = \sum_{k} \sum_{m=1}^{M} d_{k,m} g(l - k\frac{M}{2}) e^{-j2\pi \frac{m}{M} l} e^{\frac{j}{2}\pi(k+m)} \tag{1}$$

where l is the sample time index, k the symbol time index, and m the subcarrier index. $d_{k,m}$ denotes the k-th OQAM symbol on the m-th subcarrier. $g(l)$ is the impulse response of the prototype filter with a finite time duration of $L_g = KT$, where K is the overlapping factor.

Define $g_{k,m}(l) = g(l - k\frac{M}{2}) \exp(-j2\pi \frac{m}{M} l + \frac{j\pi}{2}(k+m))$ as the shifted version of $g(l)$ in both time and frequency domains. In order to keep an orthogonal condition, the filter shape $g(l)$ should be specifically designed [3]. In this paper, PHYDYAS filter with overlapping factor 4 is used.

After passing through fiber channel, the signal is distorted by chromatic dispersion, PN and ASE noise. At the receiver side, the demodulated symbol in frequency domain can be expressed as:

$$\begin{aligned} y_{k,m} &\approx H_m \sum\nolimits_l \exp(j\varphi_k) s(l) g^*_{k,m}(l)) + \sum\nolimits_l w(l) g^*_{k,m}(l) \\ &= H_m \exp(j\varphi_k) d_{k,m} \\ &\quad + jH_m \sum_{(k_1,m_1)\neq(k,m)} \exp(j\varphi_{k_1}) \xi^{k_1,m_1}_{k,m} d_{k_1,m_1} \\ &\quad + \sum\nolimits_l w(l) g^*_{k,m}(l) \end{aligned} \tag{2}$$

where H_m denotes channel frequency response of the m-th subcarrier. φ_k is the CPE of the k-th OQAM symbol. CPE is modelled as a Weiner process. And $\varphi_k - \varphi_{k-1} \sim \mathcal{N}(0, 2\pi\Delta vT/2)$. Δv denotes the combined linewidth of carrier generator and local oscillator. The product of linewidth and symbol duration $\Delta vT/2$ is called NLW. The difference of adjacent CPE values obeys zero-mean Gaussian distribution whose variance is proportional to NLW. $w(l)$ denotes ASE noise. $j\xi^{k_1,m_1}_{k,m} = \sum_l g_{k_1,m_1}(l) g^*_{k,m}(l)$ is the IMI coefficient between TF location (k, m) and (k_1, m_1). Table 1 gives the 44-neighboring IMI coefficients of symbol (k, m). For symbol $d_{k,m}$, large IMI coefficients are mostly distributed in its neighboring symbols due to the well TF localization of prototype filter. We define power ratio between neighboring interference and out-of-neighborhood interference (NOIR) as:

$$NOIR = 20 \times \log\left(\frac{|\sum_{(k_1,m_1)\in\Omega} \xi^{k_1,m_1}_{k,m} d_{k_1,m_1}|}{|\sum_{(k_1,m_1)\notin\Omega} \xi^{k_1,m_1}_{k,m} d_{k_1,m_1}|}\right) \tag{3}$$

where Ω denotes neighboring area. The average NOIRs of 8-neighborhood Ω_8, 14-neighborhood Ω_{14} and 20 neighborhood are shown in Table 1. And Ω_{14} cover all TF locations where IMI coefficients beyond 0.1. Therefore, we can make an assumption that:

$$|\sum_{(k_1,m_1)\in\Omega_{14}} \xi^{k_1,m_1}_{k,m} d_{k_1,m_1}| \gg |\sum_{(k_1,m_1)\notin\Omega_{14}} \xi^{k_1,m_1}_{k,m} d_{k_1,m_1}| \tag{4}$$

Besides, according to the slowly-varying feature of PN, we further assume that:

$$|\cos(\varphi_{k_1} - \varphi_k)| > |\sin(\varphi_{k_1} - \varphi_k)|, (k_1, m_1) \in \Omega_{14} \tag{5}$$

Based on (4) and (5), demodulated symbol in frequency domain can be rewritten as:

$$\begin{aligned} y_{k,m} &= H_m \exp(j\varphi_k)(d_{k,m} \\ &\quad + j \sum_{(k_1,m_1)\neq(k,m)} \cos(\varphi_{k_1} - \varphi_k) \xi^{k_1,m_1}_{k,m} d_{k_1,m_1}) \\ &\quad + \chi_{k,m} \\ &= H_m \exp(j\varphi_k)(d_{k,m} + j\eta) + \chi_{k,m} \end{aligned} \tag{6}$$

where the accumulated noise $\chi_{k,m}$ is expressed as:

$$\begin{aligned} \chi_{k,m} &= \sum\nolimits_l w(l) g^*_{k,m}(l) \\ &\quad - H_m \exp(j\varphi_k) \sum_{(k_1,m_1)\neq(k,m)} \sin(\varphi_{k_1} - \varphi_k) \xi^{k_1,m_1}_{k,m} d_{k_1,m_1} \end{aligned} \tag{7}$$

Note that accumulated noise $\chi_{k,m}$ is the combined noise of ASE noise and part of PN. Practically, the channel response cannot be accurately estimated. After imperfect CE, the equalized symbol can be expressed as:

$$y_{k,m} = \frac{H_m \exp(j\varphi_k)(d_{k,m} + j\eta) + \chi_{k,m}}{H_m + \Delta H} = \exp(j\varphi_k)(d_{k,m} + j\eta) + \varepsilon_{k,m} \quad (8)$$

where ΔH denotes estimation error of channel response. The PN effect in OFDM/OQAM can be divided into three terms. First, $\eta = \sum_{(k_1,m_1)\neq(k,m)} \cos(\varphi_{k_1} - \varphi_k)\xi_{k,m}^{k_1,m_1} d_{k_1,m_1}$ is the modified imaginary interference (MII) which combines effect of PN and IMI. Second term, CPE term $\exp(j\varphi_k)$, causes the rotation of both data symbol and MII in complex domain and thus causes a leakage of MII on data symbol. Mainly because of CPE and MII, the real-field orthogonality of OFDM/OQAM is destroyed. And the third, $\varepsilon_{k,m} = (\chi_{k,m} - \Delta H \exp(j\varphi_k)(d_{k,m} + j\eta))/(H_m + \Delta H)$, is equalization enhanced additive noise (EEAN) which contains ASE induced interference, minor PN effect and residual channel effect. Therefore, the performance of PNE is affected by residual channel effect, which is explored in section IV.

For PNE in OFDM/OQAM, CPE and MII are both unknown variables and nearly uncorrelated. To achieve PN estimation and compensation, both CPE and MII should be suppressed or cancelled.

III. EKF BASED BLIND PN ESTIMATION AND COMPENSATION SCHEMES

The PN can seriously degrade the system performance, and thus effective PNE schemes should be investigated. Fig. 2 presents the influence model of PN (EEAN is neglected here). As shown in Fig. 2(a), CPE only changes with time index, uncorrelated with subcarrier frequency and data symbol. At every time index k, OQAM symbols (six pointed star) on all subcarriers suffer from the same CPE.

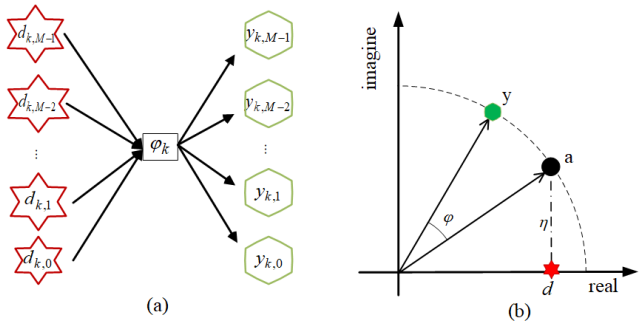

FIGURE 2. Influence model of PN. d: transmitted symbol. y: demodulated symbol. φ: PN value; η: modified imaginary interference.

From Fig. 2(b), demodulated symbol (hexagon) is rotated version of OQAM symbol (star) and its MMI η. And the rotation angle is equal to CPE. Let symbol vector $D_k = [d_{k,0}, d_{k,1}, \ldots, d_{k,M-1}]^{\mathrm{T}}$, η_k and E_k are the corresponding MMI and EEAN vector respectively, the demodulated symbol vector $Y_k = [y_{k,0}, y_{k,1}, \ldots, y_{k,M-1}]^{\mathrm{T}}$ can be expressed as:

$$Y_k = \exp(j\varphi_k)D_k + j\exp(j\varphi_k)\eta_k + \mathrm{E}_k \quad (9)$$

EKF is initially proposed for estimation of discrete-time noisy process. The filter is effective extensively even if the precise nature of noise is unknown [35]. EKF can be applied for PNE with low computation complexity [28]. For EKF based blind PNE methods, the OQAM constellation and Weiner model of PN are often used as priori information. In MSE sense, the cost function of EKF can be expressed as:

$$J_k^{\mathrm{E}}(\varphi, D) = \sum_{i=1}^{k} \lambda^{k-i} ||\Re(Y_i \exp(-j\varphi)) - D||^2 \quad (10)$$

where superscript E denotes EKF. D denotes undetermined OQAM vector.λ denotes the forgetting factor. $||*||$ denotes 2-norm of vector. $\Re$ is the *real* operator. Note that λ is proportional to the variance of EEAN, and often set to a small constant. Cost function of EKF at time k is a weighted sum in history. And PNE can be converted to double-dimensional optimization problem.

$$[\widehat{D}_k, \widehat{\varphi_k}] = \arg\min_{D\in\mathbf{O}^M} \min_{\varphi\in[-\pi,\pi]} J_k^E(\varphi, D) \quad (11)$$

To derive the EKF recursive algorithm, we firstly consider a simplified condition that transmitted OQAM symbol D_k is given. Therefore, double-dimensional problem min $[\mathrm{J}_k^E(\varphi, D)]$ is simplified to one-dimensional min$[\mathrm{J}_k^E(\varphi, D_k)]$. And conventional recursive algorithm can be derived.

$$\begin{cases} P_{k|k-1} = P_{k-1} + \pi\Delta\nu T \\ B_k = jD_k \exp(j\hat{\varphi}_{k-1}) \\ G_k = P_{k|k-1}B_k^{\mathrm{H}}/(B_k P_{k|k-1} B_k^{\mathrm{H}} + \lambda) \\ P_{k|k} = (1 - G_k B_k)P_{k|k-1} \\ \hat{\varphi}_k = \hat{\varphi}_{k-1} + G_k(Y_k - \hat{D}_k \exp(j\hat{\varphi}_{k-1})) \end{cases} \quad (12)$$

where $k|k\text{-}1$ denotes *prior* estimation. And $k|k$ (or k) denotes *a posteriori* estimation. B_k, G_k, P_k are intermediate parameter in EKF process. Note that B_k, G_k, P_k are all functions of symbol D_k which are unknown in blind PNE. Therefore, symbol D_k needs to be roughly estimated in process of EKF based PNE.

A. MODIFIED EKF

Practically, cost function is assumed to vary slowly in phase domain and fast in symbol domain. Therefore, assumptions are made that $\frac{\partial \mathrm{J}_k^E(\widehat{\varphi}_{k-1}, D_k)}{\partial\varphi} \approx 0$ and $||\frac{\partial \mathrm{J}_k^E(\widehat{\varphi}_{k-1}, D_k)}{\partial D}|| = \alpha \gg 0$. Under such assumptions, the cost function near minimum zone equals to:

$$\mathrm{J}_k^E(\varphi_{k-1}, D) \approx \mathrm{J}_k^E(\varphi_k, D_k) + \alpha||D - D_k||^2 \quad (13)$$

Based on (13), a prior estimation of symbol D_k can be obtained by previous CPE estimation value.

$$\begin{aligned}\widehat{D}_{k|k-1} &= \arg\min_{D\in\mathbf{O}^M} J_k^E(\widehat{\varphi}_{k-1}, D)\\ &\approx \arg\min_{D\in\mathbf{O}^M} ||\Re(Y_k\exp(-j\widehat{\varphi}_{k-1})) - D||^2\\ &= decision[Y_k\exp(-j\widehat{\varphi}_{k-1})]\end{aligned} \tag{14}$$

where decision is hard symbol decision operator. Decision is implemented by comparing the real part of rotated symbol with OQAM symbols and choosing the closest one. Equations (12) and (14) combine the MEKF algorithm of OFDM/OQAM, as shown in table 2 [27].

TABLE 2. MEKF algorithm.

1:	Initialization: For k=0, $\hat{\varphi}_0 = 0$, $P_0 = 0$, $Q = 2\pi\Delta v\frac{T}{2}$, $\lambda = 0.01$
2:	Computation: For k=1, 2…, do
3:	Prior estimation:
4:	Pre-decision: $D_{k\|k-1} = \text{decision}[\text{real}(Y_k\exp(-j\hat{\varphi}_{k-1}))]$
5:	Prediction State-error covariance: $P_{k\|k-1} = P_{k-1} + Q$
6:	Measurement response: $B_k = jD_{k\|k-1}\exp(j\hat{\varphi}_{k-1})$
7:	Posteriori update:
8:	Kalman gain: $G_k = P_{k\|k-1}B_k^{\mathrm{H}} / (B_kP_{k\|k-1}B_k^{\mathrm{H}} + \lambda)$
9:	State update: $\hat{\varphi}_{k\|k} = \text{real}[\hat{\varphi}_{k-1} + G_k(Y_k - D_{k\|k-1}\exp(j\hat{\varphi}_{k-1}))]$
10:	State-error covariance: $P_{k\|k} = (1 - G_kB_k)P_{k\|k-1}$
11:	Compensation decision: $D_{k\|k} = \text{decision}[\text{real}(Y_k\exp(-j\hat{\varphi}_k))]$

B. ADAPTIVE EKF

The performance of MEKF highly relies on the validity of assumption (see (13)). Once if the CPE difference is relatively large or EEAN cannot be neglected, $|\frac{\partial J_k^E(\widehat{\varphi}_{k-1}, D_k)}{\partial\varphi}| = \beta > 0$ cannot be ignored. And equation (13) cannot stand. Therefore, the cost function near phase φ_{k-1} zone can be approximated as

$$\mathrm{J}_k^E(\varphi, D) \approx \mathrm{J}_k^E(\varphi_k, D') + \alpha||D - D'||^2 + \beta||\varphi - \varphi_k||^2 \tag{15}$$

where D' denotes a wrong concave point, different from desired symbol D_k. In (15), the cost function is bivariate and priori estimation of D_k may not be correctly acquired by (14). Therefore, the error caused by priori estimation propagates in recursive loops and degrades the PN compensation performance. In EKF theory, intermediate parameter P_k reflects the variance of CPE difference at time index k, expressed as

$$\varphi_k - \widehat{\varphi}_{k-1} \sim \mathcal{N}(0, P_k) \tag{16}$$

where $\mathcal{N}$ denotes Gaussian distribution. Based on the feature of Gaussian distribution, we further assume that current CPE belongs to adaptive range $\varphi_k \in [-NP_k + \widehat{\varphi}_{k-1}, NP_k + \widehat{\varphi}_{k-1}]$ where N is a predetermined integer. Therefore, priori estimation of D_k can be modified,

$$\begin{cases}\widehat{D}_{k|k-1} = \arg\min_{D\in\mathbf{O}^M}\min_{\varphi\in\phi_k} ||\Re(Y_k\exp(-j\varphi)) - D||^2\\ \phi_k = [-NP_k + \widehat{\varphi}_{k-1}, NP_k + \widehat{\varphi}_{k-1}]\end{cases} \tag{17}$$

where ϕ_k denotes the limited phase range. Note that ϕ_k is proportional to P_k, thus adaptive to varying laser linewidth. Therefore, ϕ_k is called adaptive range here. Normally, a subset of test phases are uniformly sampled in the adaptive range for practical implementations.

$$\phi_k = \{i\Delta + \widehat{\varphi}_{k-1} | i \in Z, -NP_k < i\Delta < NP_k\} \tag{18}$$

Here, Δ is search interval and Z denotes integer set. The search interval is decided by symbol order, which has been studied in [25]. For 16 OQAM, the search interval is chosen $\pi/32$. N is a variable which decides the adaptive range. If N equal to 0, there is no adaptive range and the proposed AEKF is equal to MEKF. Theoretically, the performance of AEKF improves with the increase of N. While range parameter N and search interval Δ both predetermined, the implementation complexity of (17) only changes with intermediate parameter P_k and thus is adaptive to fluctuated laser linewidth.

In EKF theory, forgetting factor λ is proportional to the variance of measurement noise. For PNE in OFDM/OQAM, λ can be expressed as:

$$\lambda = \frac{1}{KM}\sum_k [Y_k - D_k\exp(j\varphi_k)]\cdot[Y_k - D_k\exp(j\varphi_k)]^H \tag{19}$$

In implementation of MEKF, λ is initialized by experience and may deviate from its real value. To avoid the initialization error of λ, AEKF updates the parameter according to innovation-based adaptive estimator [34].

$$\lambda_k = (1-\alpha)\lambda_{k-1} + \alpha\frac{|Y_k - D_k\exp(j\varphi_k)|^2}{M} \tag{20}$$

where α is the update constant rate and set to 0.3.

The details of AEKF are shown in Table 3. The main process of AEKF is similar to EKF. Compared to MEKF, we replace simple pre-decision in line 4 of table 2 with adaptive pre-decision in lines 3-6 of Table 3. Besides, the factor λ is updated with learning rate of 0.3 to improve robustness. Additionally, the compensation decision to recover symbols is cancelled, replaced by the optimal pre-decision (line 14).

In ideal condition, both MEKF and proposed AEKF are approximate solutions of (12). Through adaptive pre-decision, AEKF has a better robustness against varying laser linewidth, thus achieving a better performance in our expectation.

IV. RESULTS AND DISCUSSIONS

To evaluate the performance of above schemes, a 20 Gbaud 16-QAM CO-OFDM/OQAM system is numerically simulated in Monte-Carlo method. The simulation platforms are

TABLE 3. AEKF algorithm.

1: Initialization: For k=0, $\hat{\varphi}_0 = 0$, $P_0 = 0$, $Q = 2\pi\Delta v \frac{T}{2}$, $\Delta = \pi/32$

2: Computation: For k=1, 2…, do

3: Prior estimation:

4: Adaptive Pre-decision:

5: Adaptive range: $aset = \hat{\varphi}_k + \Delta * \text{round}([-14P_k/\Delta, 14P_k/\Delta])$

Optimal pre-decision:

6: $$D_{k|k-1} = \underset{D\in O^M}{\text{argmin}} \min_{\varphi_t \in aset} \| \text{real}[Y_k \exp(-j\varphi_t)] - D \|^2$$

7: Prediction State-error covariance: $P_{k|k-1} = P_{k-1} + Q$

8: Measurement response: $B_k = jD_{k|k-1}\exp(j\hat{\varphi}_{k-1})$

9: Posteriori update:

10: Kalman gain: $G_k = P_{k|k-1}B_k^{\mathrm{H}} / (B_k P_{k|k-1} B_k^{\mathrm{H}} + \lambda_{k-1})$

11: State update: $\hat{\varphi}_{k|k} = \text{real}[\hat{\varphi}_{k-1} + G_k(Y_k - D_{k|k-1}\exp(j\hat{\varphi}_{k-1}))]$

12: State-error covariance: $P_{k|k} = (1 - G_k B_k)P_{k|k-1}$

13: Measure variance (forgetting factor):

$$\lambda_k = 0.7\lambda_{k-1} + 0.3 * \text{mean}[(Y_k - D_{k|k-1}\exp(j\hat{\varphi}_k))^2]$$

14: Compensation decision: $D_{k|k} = D_{k|k-1}$

Matlab and VPI. Over 2^{18} random bits are used as information sources. After 16-ary QAM, the data symbols are mapped onto TF plane. In optical domain, the center frequency of lasers is 193.1 THz and Standard Single Mode Fiber (SSMF) is used for transmission. At receiver side, the signal is firstly demodulated by analysis filter bank. Then Modified Least Square-2 (M-LS-2) method with 9 time-slot train sequence is used for CE [36]. After CE, PNE and compensation recover OQAM symbol. And then symbol de-mapping recovers the bits. The recovered bits are compared with transmitted bits to estimate bit error rate (BER). The performances of three blind methods (MBPS-FL [24], MEKF [28], AEKF) and one pilot-aided method (PEKF [22]) are compared. 4 pilot subcarriers pilot-aided are loaded with random OQAM symbols and their 8 neighboring subcarriers are loaded with zero-symbol to cancel MMI in PEKF scheme.

Before we compare the performance of different PNE schemes, we first study the effect of adaptive range on AEKF. Fig. 3 shows BER of AEKF at different adaptive ranges, at linewidth of 500 kHz, optical signal to noise ratio (OSNR) of 20 dB, in back to back (BTB) configuration. $\phi_k = [-0P_k, 0P_k] + \hat{\varphi}_{k-1}$ means no adaptive range, under such condition AEKF similar to MEKF. As adaptive range extends from $[-0P_k, 0P_k]$ to $[-20P_k, 20P_k]$, BER of AEKF shows a ladder-type decent. This is because the set of test phases is extracted by discretizing the adaptive range. When the change of adaptive range is less than discrete phase interval Δ, the number of test phases in (18) cannot increase and the BER stays unchanged. Once the change of adaptive range exceeds phase interval, the number of test phases increase and the BER performance shows a sudden improvement. From Fig. 3, AEKF can provide its best performance with adaptive range higher than $[-10P_k, 10P_k]$. To ensure a reliable performance under a larger linewidth, we choose an ample range of $[-14P_k, 14P_k]$ for following simulations.

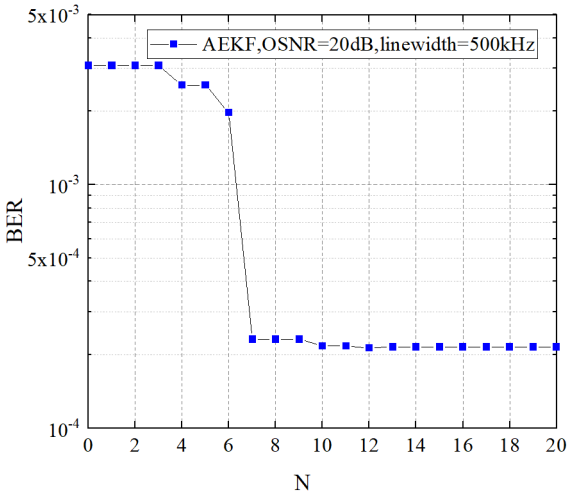

FIGURE 3. BER versus adaptive range ([-N × P, N × P]), at 20 dB OSNR, linewidth of 500 kHz.

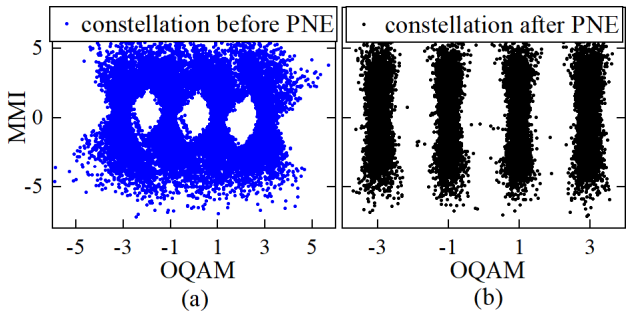

FIGURE 4. OQAM symbol constellation comparisons in the PNE process. (a) before PNE (b) after PNE.

To eliminate the effect of fiber, we then study PNE performance in BTB transmission. Fig. 4 shows the changes of constellation in AEKF PNE process which directly proves the PNE's effect for symbol recovery. Before PNE, the 16-OQAM symbols overlap each other due to PN-caused rotation and EEAN noise. After PNE, the symbols are mostly separated and relatively easy to classify. Fig. 5 further gives the performance comparison of AEKF and other EKF schemes in terms of BER against OSNR under different linewidth. Three subfigures 5(a), 5(b) and 5(c) correspond to 200 kHz, 500 kHz and 1 MHz, respectively. In all the three figures, the 'Theory' curves, that the best performance of our simulation system, are based on referential system configuration without PN. The short dash lines denote 7% Forward Error Correction (FEC) limit (3.8×10^{-3}). When BER under the limit, the system is considered to achieve a reliable communication. The theoretical OSNR required for FEC limit is about 14.1 dB. In Fig. 5(a) and 5(b), the performance of AEKF is similar to MBPS-FL. With OSNR increasing, BER of AEKF decreases to 7% FEC limit at about 15 dB, faster than those of PEKF and MEKF. When linewidth up to 1 MHz (Fig. 5(c)), the performance of MEKF rapidly degrades. The BER is almost unchanged and cannot reach 3.8×10^{-3}. When

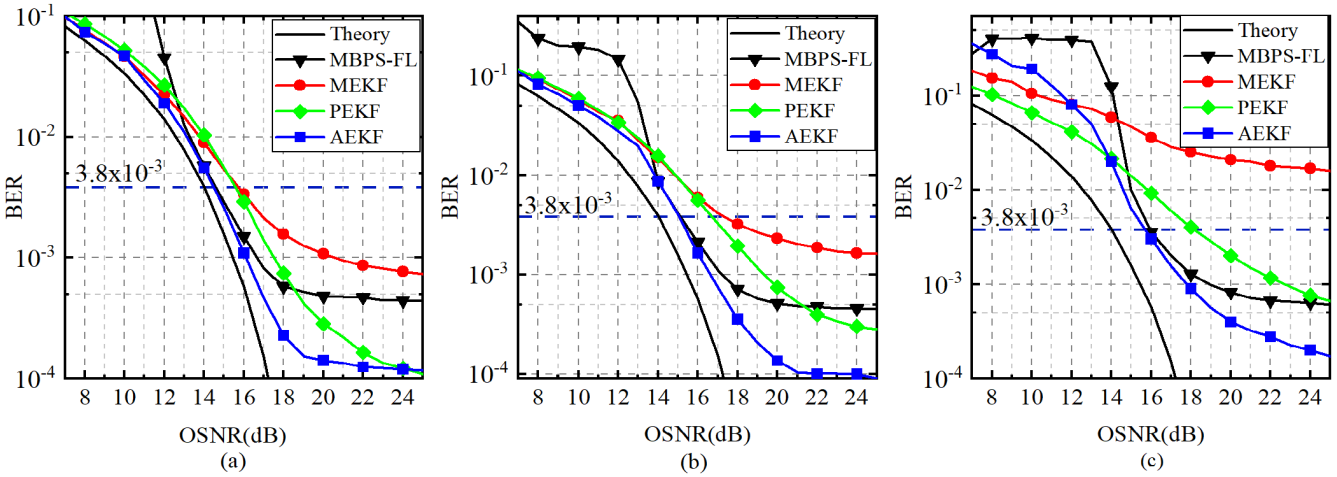

FIGURE 5. BER versus OSNR at linewidth (a) 200 kHz (b) 500 kHz (c) 1MHz.

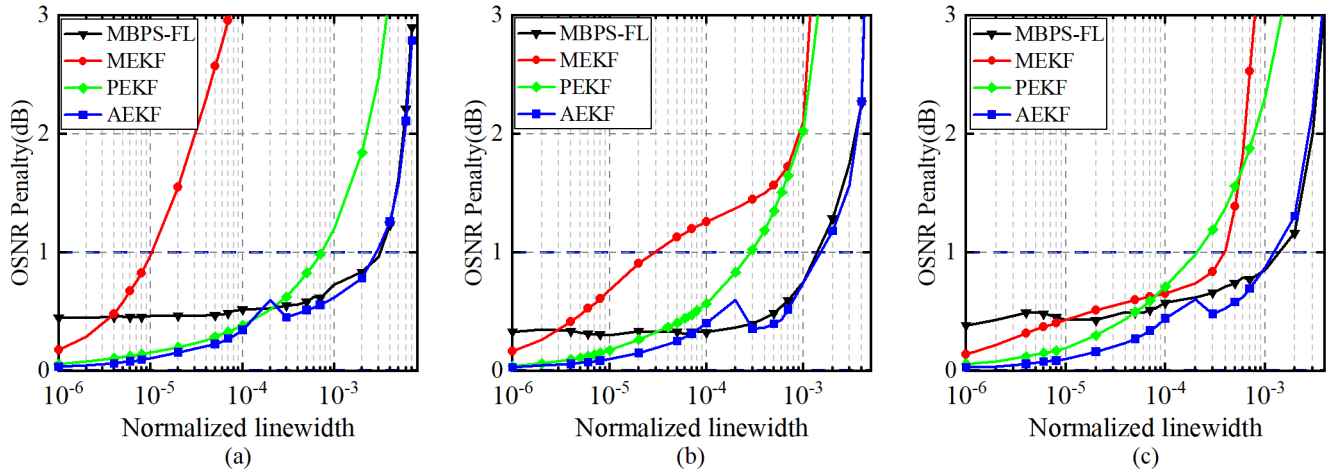

FIGURE 6. OSNR penalty against NLW with different number of subcarriers (a)64 (b)128 (c)256.

OSNR is lower than 13 dB, the BER of MBPS-FL fluctuates over 0.2 and BER of AEKF is also higher than PEKF. This is because AEKF and MBPS-FL cannot well average the EEAN' influence. Large EEAN cause estimation error which propagates in recursive loops, thus leading to a damage to BER. At OSNR higher than 14 dB, AEKF still provides a better performance, achieving a 3.8×10^{-3} BER at about 15 dB. The result shows the superiority of AEKF at high linewidth without fiber.

Further we evaluate the flexibility of schemes by comparing PN tolerance under different subcarrier allocations. Fig. 6 shows the OSNR penalty of all methods versus NLW with different number of subcarriers. Here, OSNR penalty is the extra OSNR with respect to theoretical OSNR needed to achieve BER of 3.8×10^{-3}. As shown in Fig. 5, the required OSNR is 14.1 dB. NLW is equal to $\Delta\nu T/2$. Fig. 6(a) is OSNR penalty versus NLW of 64 subcarriers, Fig. 6(b) 128 subcarriers and Fig. 6(c) 256 subcarriers. All the subcarrier numbers are selected powers of 2 for efficient fast Fourier transform based modulation. Note that the symbol rate keeps constant while subcarrier number changes. In all the three figures, the dash horizontal lines denote 1 dB OSNR penalty, which is accepted as PN tolerance threshold for comparison. With subcarrier number increasing, PN tolerance of MEKF increases from 1×10^{-5} of 64 subcarriers to 4×10^{-4} of 256 subcarriers. This is mainly because, in every recursive loop, the equalization of MEKF becomes stronger with more data symbols used. The PN tolerance of PEKF is decreasing from 6×10^{-4} of 64 subcarriers to 2×10^{-4} of 256 subcarriers because the pilot to subcarrier ratio decreases from 4/64 to 4/256. In all the three figures, there is a sub-peak the OSNR penalty of AEKF at NLW of 2×10^{-4}. This is because the set of test phases is extracted by discretizing the adaptive range. As NLW increases to 2×10^{-4}, the adaptive range is also increasing because adaptive range is proportional to intermediate parameter P_k in (17) and P_k is positively

correlated to NLW. However, the increase of adaptive range is less than discrete phase interval Δ and the OSNR penalty increases with NLW. As NLW exceeds 2×10^{-4}, the change of adaptive range exceeds phase interval and the number of test phases increase. Therefore, the performance shows a sudden improvement and OSNR penalty shows a decent at NLW of 3×10^{-4}. Obviously, the tolerances of AEKF and MBPS-FL outperform those of MEKF and PEKF, stable around 1.5×10^{-3}. This fact further shows the advantage of AEKF in terms of PN tolerance.

Next, we simulate the PNE performance at 80 Km transmission of SSMF. Fig. 7(a) shows the BER evolution with OSNR at 200 kHz linewidth (NLW of 6.4×10^{-4}). The five-star curve denotes the performance only with CE. when there is no PN. The CE method cannot fully compensate the effect of SSMF channel, causing a OSNR penalty of 2.7 dB. Among the four PNE methods, AEKF and MBPS-FL provide the best performance with additional 0.8 dB OSNR penalty while MEKF with 2.3 dB OSNR penalty. And PEKF cannot achieve reliable transmission below 25 dB OSNR. Fig. 7(b) shows the additional OSNR penalty caused by PNE at different NLWs. The NLW tolerances of four methods all degrade compared to BTB transmission in Fig. 6(b). The tolerance of MBPS-FL is 7×10^{-4}, AEKF 8×10^{-4}, MEKF 1.5×10^{-5} and PEKF 4×10^{-5}.

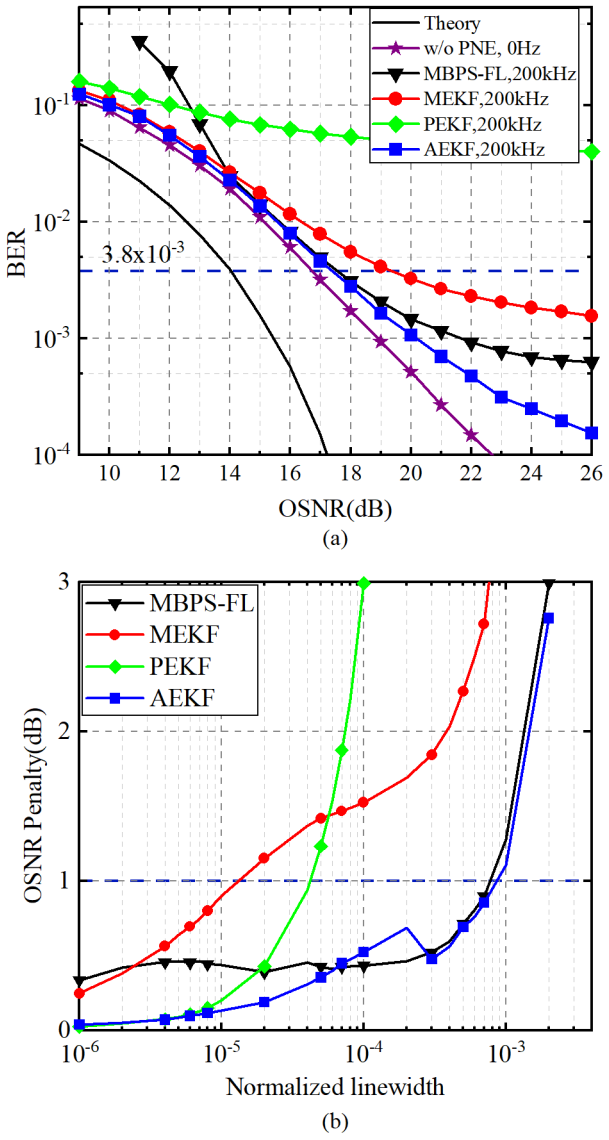

FIGURE 7. PNE performance at 80Km transmission (a) BER versus OSNR at 200 kHz (b) OSNR penalty caused by PNE versus NLW.

Then we analyze the robustness of different PNE schemes against fiber dispersion. The fiber loss is perfectly compensated by EDFA. Fig. 8 shows the BER versus transmission fiber length with different PNE schemes at OSNR of 25dB. The black line denotes performance only with CE at 0 Hz linewidth. Obviously, with M-LS-2 CE method employed, the system can support the longest transmission distance of 550 Km. However, residual channel effect and laser PN certainly lead to a reduction of the transmission distance. Here, the reduction of transmission distance with respect to theoretical distance is called transmission distance penalty.

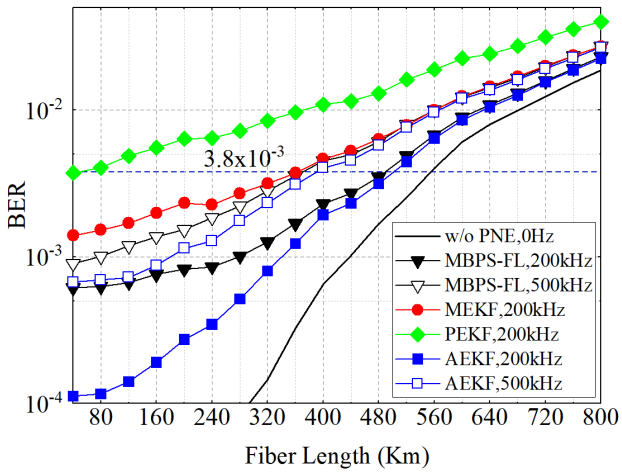

FIGURE 8. PNE performance versus transmission length at OSNR of 25dB.

At linewidth of 200 kHz, AEKF and MBPS-FL have the best robustness against fiber effect with 60 Km transmission distance penalty while MEKF with 200 Km penalty. The PEKF (with 4 pilot subcarriers and random pilot symbols) is sensitive to fiber and cannot support fiber transmission over 80 Km. At linewidth of 500 kHz, transmission distance penalties of AEKF and MBPS-FL further degrade to 160 Km and 180 Km.

Finally, we compare the computation complexity of all schemes. Normally, the complexity of PNE is measured by counting the number of real multiplications, real additions and decision operators per OQAM symbol. And decision operator is a major factor for complexity. Table 4 gives complexity analysis in terms of both estimation and compensation. The complexity of PEKF is the lowest because only two pilot symbol are used in every loop. Complexity of

TABLE 4. Complexity comparison by operator. B: number of test phase; M: number of subcarriers.

Algorithm	Real Multiplication	Real Addition	Decision
MBPS-FL	2BM	BM	BM
MEKF	7M	3M	2M
PEKF	12	12	M

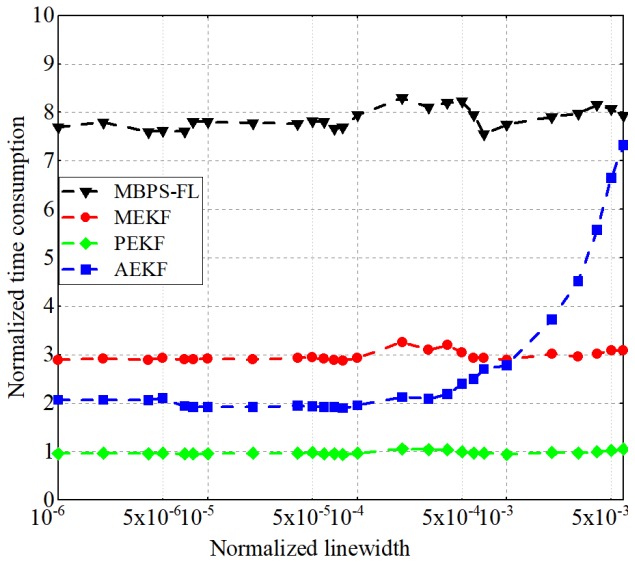

FIGURE 9. Complexity comparison by the time consumption.

MBPS-FL is much higher due to extensive search in phase domain and symbol domain. Complexity of MEKF lies in the middle. However, the complexity of AEKF cannot be directly compared by operator number because it is highly correlated to NLW. Therefore, time consumptions of different schemes are compared. Over 400 repeated implementations for each schemes are executed in the same machine on Matlab platform. Fig. 9 shows the evolution of time consumption at different NLWs. The averaging time consumption of PEKF is 0.0065 s, used as the unit. At NLW lower than 3×10^{-4}, complexity of AEKF remains nearly unchanged between that of PEKF and MEKF. As NLW continues increasing, the complexity of AEKF increases like a linear process. At NLW of 5×10^{-3} (linewidth of 700 kHz), the complexity of AEKF is equal to that of MBPS-FL. Fig. 9 still shows the advantage of AEKF in terms of reasonable usage of computation power.

V. CONCLUSION

In this paper, the performances of MBPS-FL, MEKF, PEKF and the proposed AEKF are demonstrated by numerical analysis. The results show that the BER performance of AEKF is better than that of MBPS-FL and MEKF at high OSNR. Under different subcarrier allocation (64, 128, 256 subcarriers), AEKF has a stable NLW tolerance over 1.5×10^{-3} and possesses a lower computation complexity than MEKF and MBPS-FL when NLW lower than 1×10^{-3}. At commercial laser linewidth of 200 kHz, AEKF's time complexity is about 1/3 of MBPS-FL's complexity, lower than MEKF's complexity. Besides, AEKF has strong tolerance against fiber effect, supporting longer distance transmission than MEKF. In conclusion, AEKF algorithm makes CO-OFDM/OQAM system strong in robustness against fiber effect, subcarrier allocation and laser linewidth. Therefore, AEKF is a promising PNE scheme for CO-OFDM/OQAM system in dynamic networks to provide moderate high flexibility and low complexity while assuring reliable performance.

REFERENCES

[1] R. Nissel, S. Schwarz, and M. Rupp, "Filter bank multicarrier modulation schemes for future mobile communications," *IEEE J. Sel. Areas Commun.*, vol. 35, no. 8, pp. 1768–1782, Aug. 2017.

[2] B. Saltzberg, "Performance of an efficient parallel data transmission system," *IEEE Trans. Commun. Technol.*, vol. 15, no. 6, pp. 805–811, Dec. 1967.

[3] M. Bellanger, D. LeRuyet, D. Roviras, and M. Terré. (2010). *FBMC Physical Layer: A Primer*. [Online]. Available: http://www.ictphydyas.org/

[4] C. Li and Q. Yang, "Optical OFDM/OQAM for the future fiber-optics communications," *Procedia Eng.*, vol. 140, pp. 99–106, Jan. 2016.

[5] M. Bi, L. Zhang, L. Liu, G. Yang, R. Zeng, S. Xiao, Z. Li, and Y. Song, "Experimental demonstration of the OQAM-OFDM-based wavelength stacked passive optical networks," *Opt. Commun.*, vol. 394, pp. 129–134, Jul. 2017.

[6] C. Li, Q. Yang, and M. Luo, "100.29-Gb/s direct detection optical OFDM/OQAM 32-QAM signal over 880?km SSMF transmission using a single photodiode," *Opt. Lett.*, vol. 40, no. 7, pp. 1185–1188, 2015.

[7] Z. Xuebing, Z. Li, and C. Li, "100-Gb/s DDO-OFDM/OQAM transmission over 320-km SSMF with a single photodiode," in *Proc. IEEE Conf. Opt. Fibre Technol.*, Jul. 2014, pp. 611–612.

[8] J. He, B. Li, L. Deng, M. Tang, L. Gan, S. Fu, P. P. Shum, and D. Liu, "Experimental investigation of inter-core crosstalk tolerance of MIMO-OFDM/OQAM radio over multicore fiber system," *Opt. Express*, vol. 24, no. 12, 2016, Art. no. 13418.

[9] T. Pollet, M. Van Bladel, and M. Moeneclaey, "BER sensitivity of OFDM systems to carrier frequency offset and Wiener phase noise," *IEEE Trans. Commun.*, vol. 43, nos. 2–4, pp. 191–193, Feb. 1995.

[10] L. Tomba, "On the effect of Wiener phase noise in OFDM systems," *IEEE Trans. Commun.*, vol. 46, no. 5, pp. 580–583, May 1998.

[11] S. Wu and Y. Bar-Ness, "OFDM systems in the presence of phase noise: Consequences and solutions," *IEEE Trans. Commun.*, vol. 52, no. 11, pp. 1988–1996, Nov. 2004.

[12] F. Munier, T. Eriksson, and A. Svensson, "An ICI reduction scheme for OFDM system with phase noise over fading channels," *IEEE Trans. Commun.*, vol. 56, no. 7, pp. 1119–1126, Jul. 2008.

[13] Q. Zou, A. Tarighat, and A. H. Sayed, "Compensation of phase noise in OFDM wireless systems," *IEEE Trans. Signal Process.*, vol. 55, no. 11, pp. 5407–5424, Nov. 2007.

[14] R. A. Casas, S. L. Biracree, and A. E. Youtz, "Time domain phase noise correction for OFDM signals," *IEEE Trans. Broadcast.*, vol. 48, no. 3, pp. 230–236, Sep. 2002.

[15] D. Petrovic, W. Rave, and G. Fettweis, "Effects of phase noise on OFDM systems with and without PLL: Characterization and compensation," *IEEE Trans. Commun.*, vol. 55, no. 8, pp. 1607–1616, Aug. 2007.

[16] N. N. Tchamov, J. Rinne, A. Hazmi, M. Valkama, V. Syrjala, and M. Renfors, "Enhanced algorithm for digital mitigation of ICI due to phase noise in OFDM receivers," *IEEE Wireless Commun. Lett.*, vol. 2, no. 1, pp. 6–9, Feb. 2013.

[17] M.-K. Lee, K. Yang, and K. Cheun, "Iterative receivers based on subblock processing for phase noise compensation in OFDM systems," *IEEE Trans. Commun.*, vol. 59, no. 3, pp. 792–802, Mar. 2011.

[18] F. Rottenberg, T.-H. Nguyen, S.-P. Gorza, F. Horlin, and J. Louveaux, "ML and MAP phase noise estimators for optical fiber FBMC-OQAM systems," in *Proc. IEEE Int. Conf. Commun. (ICC)*, May 2017, pp. 1–6.

[19] A. Ishaque and G. Ascheid, "On the sensitivity of SMT systems to oscillator phase noise over doubly-selective channels," in *Proc. IEEE Wireless Commun. Netw. Conf. (WCNC)*, Mar. 2015, pp. 545–550.

[20] K. Ikeuchi, M. Sakai, and H. Lin, "Compensation of phase noise in OFDM/OQAM systems," in *Proc. IEEE 86th Veh. Technol. Conf. (VTC-Fall)*, Sep. 2017, pp. 1–5.
[21] T. T. Nguyen, S. T. Le, R. Nissel, M. Wuilpart, L. Van Compernolle, and P. Megret, "Pseudo-pilot coding based phase noise estimation for coherent optical FBMC-OQAM transmissions," *J. Lightw. Technol.*, vol. 36, no. 14, pp. 2859–2867, Jul. 15, 2018.
[22] B. You, L. Yang, F. Luo, S. Yang, D. Chen, Y. Ni, B. Li, and D. Liu, "Pilot-based extended Kalman filter for phase noise estimation in CO-FBMC/OQAM systems," *Opt. Commun.*, vol. 443, pp. 116–122, Jul. 2019.
[23] B. You, L. Yang, F. Luo, S. Fu, S. Yang, B. Li, and D. Liu, "Joint carrier frequency offset and phase noise estimation based on pseudo-pilot in CO-FBMC/OQAM system," *IEEE Photon. J.*, vol. 11, no. 1, pp. 1–11, Feb. 2019.
[24] S. T. Le, P. A. Haigh, A. D. Ellis, and S. K. Turitsyn, "Blind phase noise estimation for CO-OFDM transmissions," *J. Lightw. Technol.*, vol. 34, no. 2, pp. 745–753, Jan. 15, 2016.
[25] T.-H. Nguyen, J. Louveaux, S.-P. Gorza, and F. Horlin, "Simple feedforward carrier phase estimation for optical FBMC/OQAM systems," *IEEE Photon. Technol. Lett.*, vol. 28, no. 24, pp. 2823–2826, Dec. 15, 2016.
[26] T.-H. Nguyen, S.-P. Gorza, J. Louveaux, and F. Horlin, "Lowcomplexity blind phase search for filter bank multicarrier Offset-QAM optical fiber systems," in *Advanced Photonic*. Washington, DC, USA: OSA, Jul. 2016, p. SpW2G.2. [Online]. Available: http://www.osapublishing.org/abstract.cfm?URI=SPPCom-2016-SpW2G.2
[27] X. Yan, C. Cao, W. Zhang, X. Zeng, Z. Feng, Z. Wu, X. Su, and T. Wang, "Low-complexity carrier phase estimation for M-ary quadrature amplitude modulation optical communication based on dichotomy," *Opt. Express*, vol. 28, no. 17, pp. 25263–25277, Aug. 2020.
[28] T.-H. Nguyen and C. Peucheret, "Kalman filtering for carrier phase recovery in optical offset-QAM nyquist WDM systems," *IEEE Photon. Technol. Lett.*, vol. 29, no. 12, pp. 1019–1022, Jun. 15, 2017.
[29] J. C. M. Diniz, Q. Fan, S. M. Ranzini, F. N. Khan, F. D. Ros, D. Zibar, and A. P. T. Lau, "Low-complexity carrier phase recovery based on principal component analysis for square-QAM modulation formats," *Opt. Express*, vol. 27, no. 11, pp. 15617–15626, May 2019.
[30] J. Zhao, "Format-transparent phase estimation based on KL divergence in coherent optical systems," *Opt. Express*, vol. 28, no. 14, pp. 20016–20031, Jul. 2020.
[31] K. Roberts and C. Laperle, "Flexible transceivers," in *Proc. Eur. Conf. Exhib. Opt. Commun.*, 2012, pp. 1–3.
[32] K. Roberts, "Flexible optical transceivers," *Proc. SPIE*, vol. 10561, Jan. 2018, Art. no. 1056104.
[33] I. Hashlamon, "A new adaptive extended Kalman filter for a class of nonlinear systems," *J. Appl. Comput. Mech.*, vol. 6, no. 1, pp. 1–12, 2020.
[34] D. Xile, Z. Caiping, and J. Jiuchun, "Evaluation of SOC estimation method based on EKF/AEKF under noise interference," *Energy Procedia*, vol. 152, pp. 520–525, Oct. 2018.
[35] R. E. Kalman, "A new approach to linear filtering and prediction problems," *J. Basic Eng.*, vol. 82, no. 1, p. 35, 1960.
[36] Z. Jian, "Channel estimation in DFT-based offset-QAM OFDM systems," *Opt. Express*, vol. 22, no. 21, pp. 25651–25662, 2014.

XIAOBO WANG received the B.S. degree in information engineering from Tianjin University, Tianjin, China, in 2018. He is currently pursuing the M.Sc. degree with the School of Optical and Electronic information, Huazhong University of Science and Technology, Wuhan, China.

His research interest includes fiber optic communications.

LIU YANG received the B.S. degree in electronics science and technology from Shandong University, Jinan, China, in 2012, and the Ph.D. degree in photoelectric information engineering form the Huazhong University of Science and Technology, Wuhan, China, in 2017.

He is currently a Postdoctoral Fellow with the Huazhong University of Science and Technology. His research interests include optical communications, optical algorithms, and optical interconnection devices.

FENGGUANG LUO received the B.S., M.S., and Ph.D. degrees from the Huazhong University of Science and Technology (HUST), China, in 1984, 1989, and 1999, respectively.

From 1984 to 1986, he spent two years at the Wuhan Research Institute of Posts and Telecommunications, China. Since 1989, he has been working with the School of Optical and Electronic Information, Huazhong University of Science and Technology. From 1997 to 1998, he worked with the Department of Electronic Engineering, City University of Hong Kong, as a Senior Visiting Scholar. His research interests include optical communications, optical switching, optoelectronic devices, and optical interconnection.

SHUAILONG YANG received the B.S. degree in optical information science and technology from the Changchun University of Science and Technology, Jilin, China, in 2016. He is currently pursuing the Ph.D. degree with the College of Optics and Electronic Information, Huazhong University of Science and Technology, Wuhan, China.

His research interest includes short-range optical communications.

YUTING DU received the B.S. degree in optical and electronic information from the Huazhong University of Science and Technology, Wuhan, China, in 2018, where he is currently pursuing the M.S. degree.

His research interest includes free space optical communications.